Anchored plasticity opens doors for selective inhibitor design in nitric oxide synthase

Elsa D. Garcin, Andrew S. Arvai, Robin J. Rosenfeld, Matt D. Kroeger, Brian R. Crane, Gunilla Andersson, Glen Andrews, Peter J. Hamley, Philip R. Mallinder, David J. Nicholls, Stephen A. St-Gallay, Alan C. Tinker, Nigel P. Gensmantel, Antonio Mete, David R. Cheshire, Stephen Connolly, Dennis J. Stuehr, Anders Åberg, Alan V. Wallace, John A. Tainer, Elizabeth D. Getzoff.

SUPPLEMENTARY FIGURES

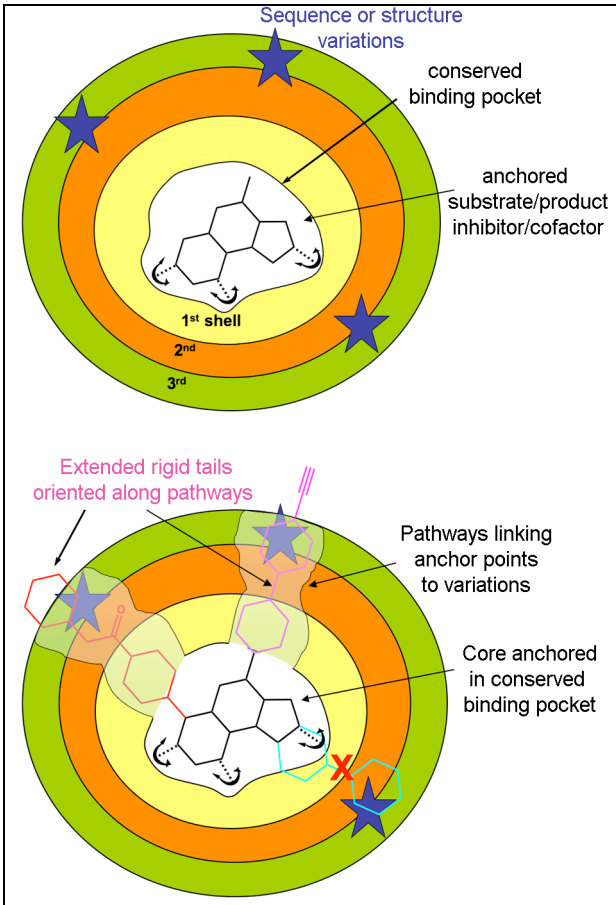

Supplementary Figure 1 Anchored plasticity approach. Schematic of the anchored plasticity approach that can be used broadly for enzyme families with conserved binding pockets. An inhibitor core is anchored in a conserved binding pocket (white). Rigid bulky substituents (red, magenta, blue) extend along pathways (shaded) that link anchor points (anchors) to variations (stars). Variations in second-shell (orange) and third-shell (green) residues are identified outside the conserved binding pocket (first-shell, yellow)

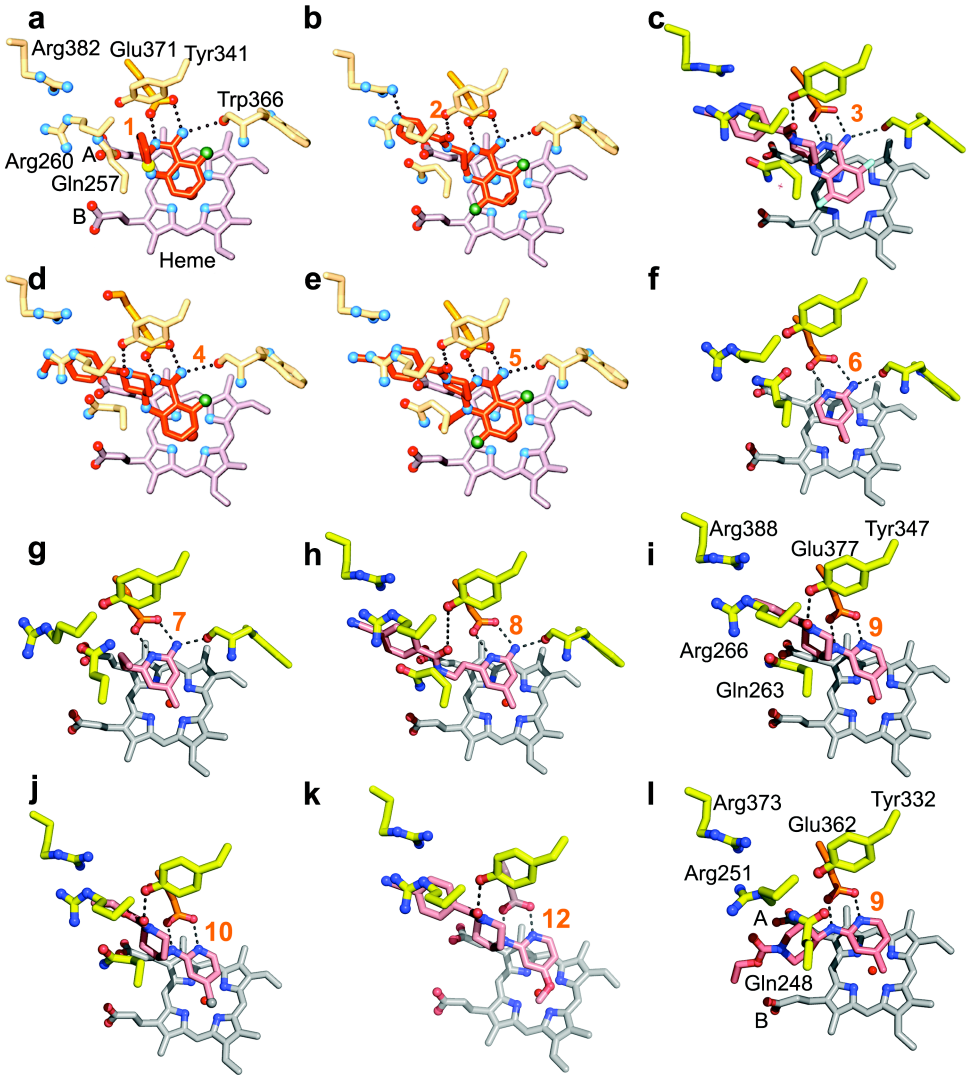

Supplementary Figure 2 Quinazoline and aminopyridine binding to iNOS and eNOS. (**a**-**e**) Simplified active-site views of x-ray structures of murine iNOSox with quinazoline compounds **1**-**5**. (**f**-**k**) Aminopyridines **6**-**12** binding to murine iNOSox and human iNOSox (**9**). (**l**) Aminopyridine **9** binding to bovine eNOSox. The simplified views with key hydrogen bonds (dots) from inhibitor to NOS residues reveal similar binding modes for all quinazoline and aminopyridine inhibitors in iNOS.

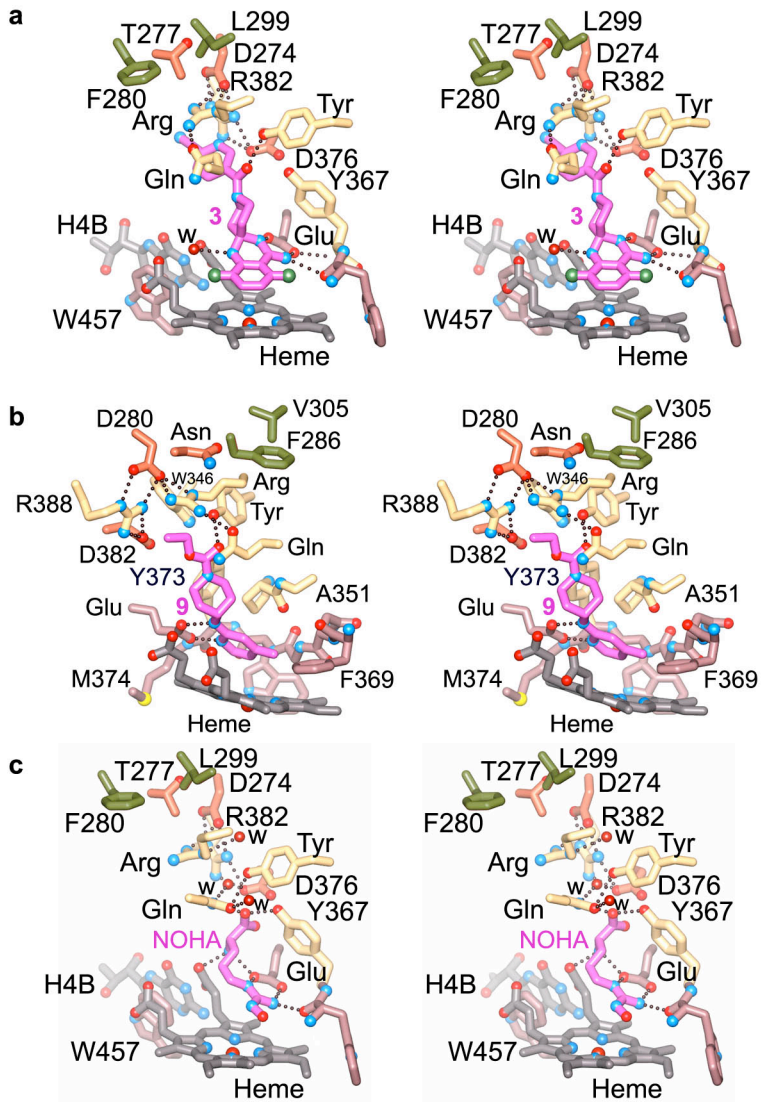

Supplementary Figure 3 Inhibitor-associated conformational changes in first- and second-shell residues in iNOSox. (**a**) Spirocyclic quinazoline compound **3** (pink) binding to murine iNOS in the Gln specificity pocket (yellow) correlates with side-chain rotation of first-shell residues **Gln** (Gln-open conformation), **Arg**, and Arg382/388. Inhibitor binding further modifies the hydrogen bond network with second-shell (orange) residues. (**b**) The binding mode of selective aminopyridine **9** (pink) to human iNOSox is very similar to that of compound **3** in murine iNOSox (**a**). Inhibitor **9** binding further induces conformational changes in second-shell **Asn**,

which fits in a hydrophobic pocket created by third-shell Val305 and Phe286 (green). (**c**) Reaction intermediate NOHA (pink) binds to murine iNOS[1] via direct interactions with residues forming the active-site heme pocket (peach). The carboxylate moiety of NOHA hydrogen bonds to first-shell Tyr367/373 and **Gln** (yellow). **Gln** hydrogen bonds to **Tyr** and is in the Gln-closed conformation. All figures are stereoviews.

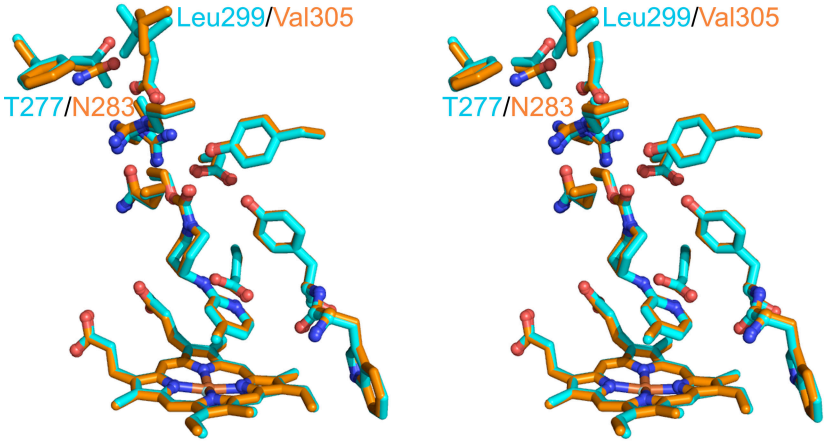

Supplementary Figure 4 Compound **9** binding to murine (blue) and human (orange) iNOSox. Stereoview of compound **9** binding similarly to both murine and human iNOSox orthologs, with a 0.2 Å r.m.s. deviation (vs. comparable r.m.s. deviation of 0.1 Å between four crystallographic distinct murine iNOSox molecules). In murine iNOSox, the cascade of conformational changes upon inhibitor binding ends at Thr277.

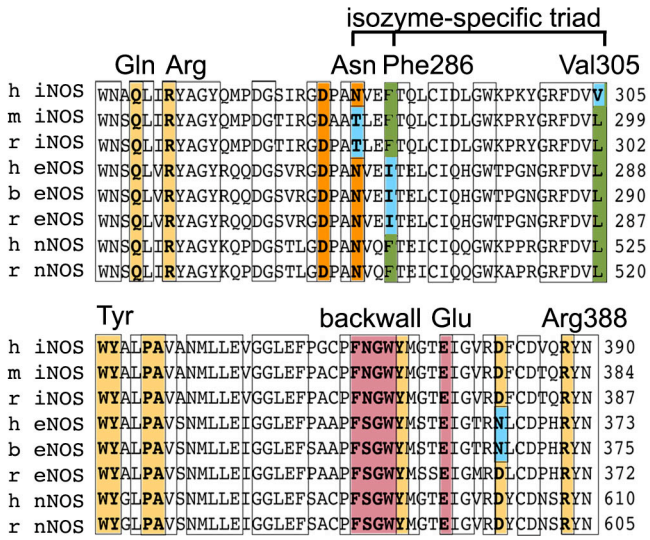

Supplementary Figure 5 Amino-acid sequence alignment for NOS isozymes. Residues forming the active site (pink) include the backwall (FNGW) residues and invariant **Glu**. Invariant first-shell residues include **Gln**, **Arg**, Arg388, and **Tyr**, isozyme-specific second-shell **Asn,** and third-shell Phe286 and Val305 are indicated and colored according to **Fig. 2**. Strictly conserved residues among the three isoforms are boxed and isozyme-specific residues are highlighted in blue. Key residues are indicated above the alignment (human iNOS numbering). Sequences are shown for human (h), murine (m), rat (r), and bovine (b) NOS isozymes.

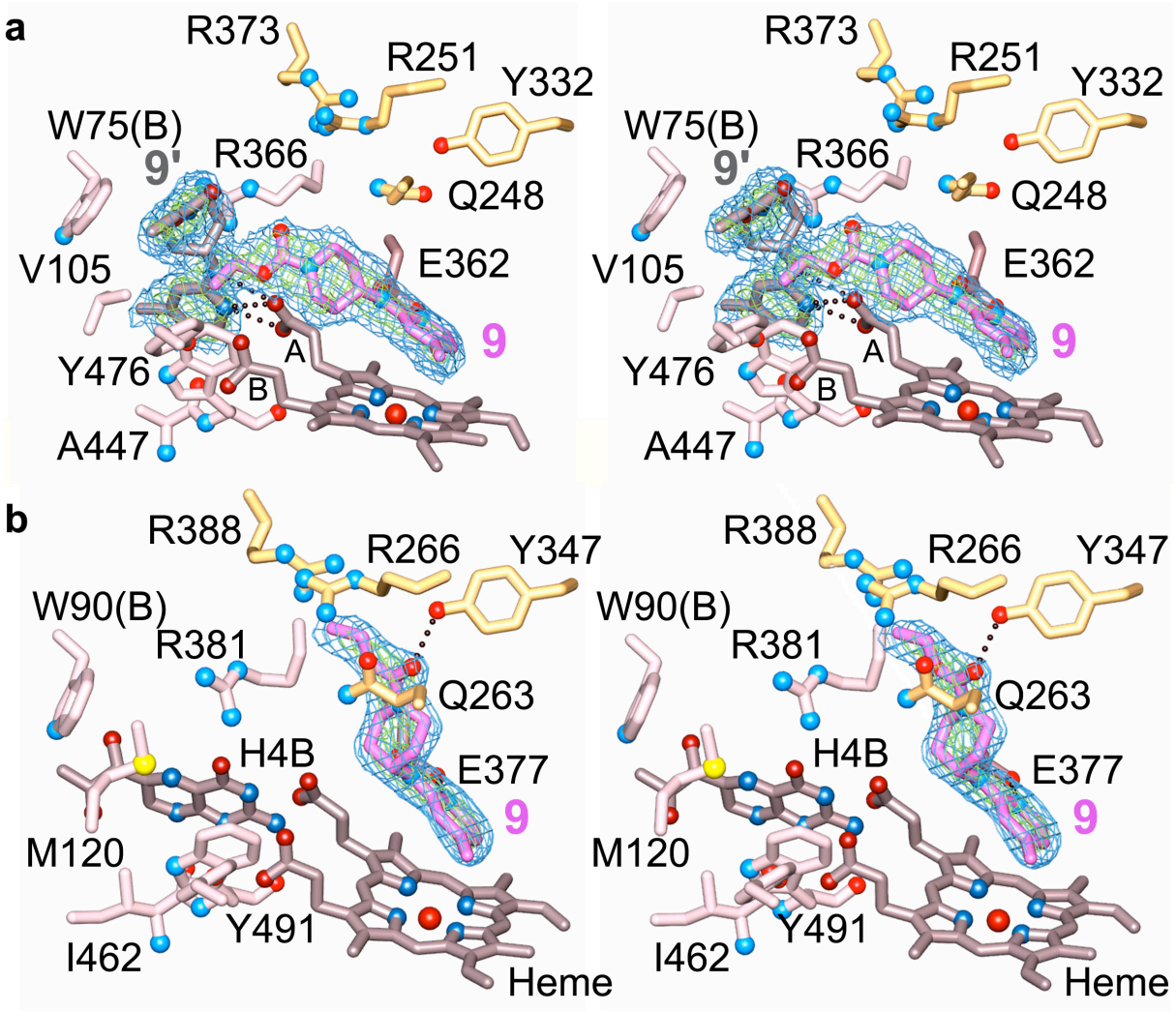

Supplementary Figure 6 Selective aminopyridine compound **9** binding to eNOS versus iNOS. Stereoview showing that the binding mode of compound **9** is different in (**a**) bovine eNOSox and (**b**) human iNOSox. Simulated-annealing 3Fo-2Fc inhibitor-omit maps are contoured at 1 σ and 3 σ for eNOS and 2 σ and 5 σ for iNOS, (blue and green, respectively). Key inhibitor-protein hydrogen bonds (dots) are shown. The eNOSox pterin site binds a second inhibitor molecule (labeled **9'**). Key residues involved in H4B or compound **9'** binding are shown.

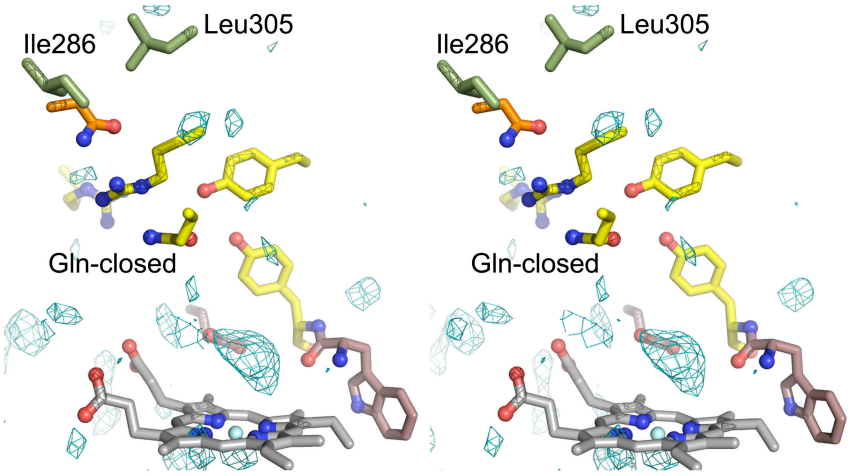

Supplementary Figure 7 X-ray structure of the human iNOSox double mutant. Stereoview showing that the active site of the human iNOSox F286I/V305L double mutant is empty and the Gln pocket is not observed. The Fo-Fc map is contoured at 3 σ (blue mesh).

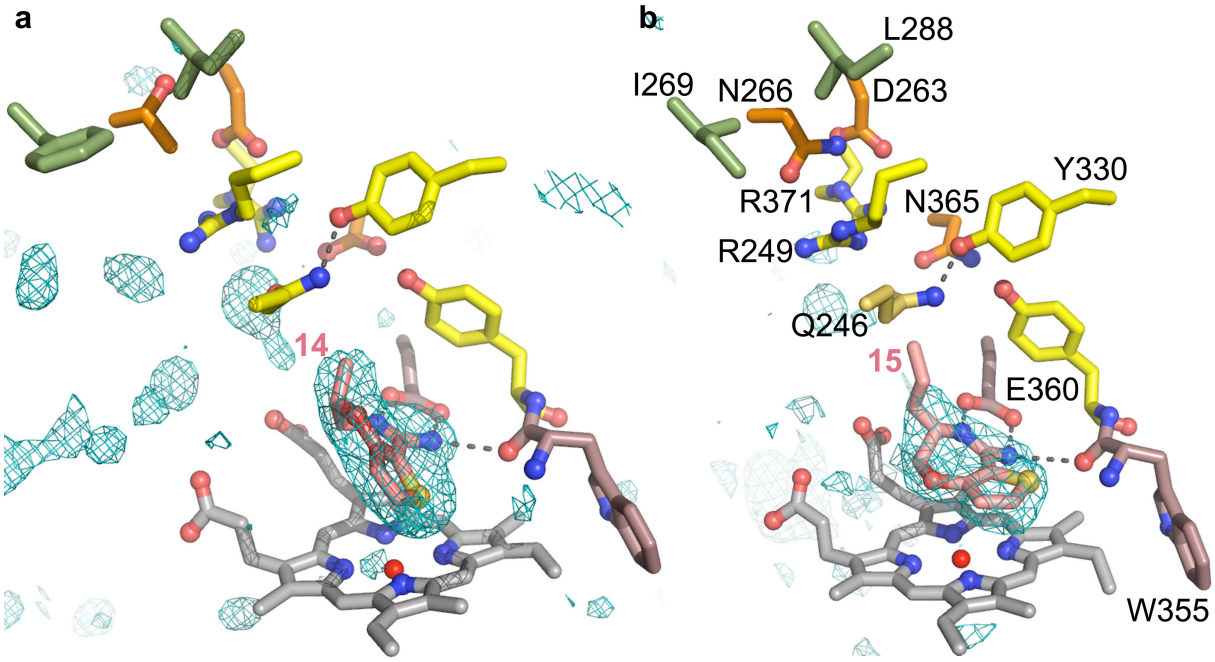

Supplementary Figure 8 Bicyclic thienooxazepine inhibitors binding to iNOS and eNOS. The binding modes of compounds **14** and **15** (pink) are different in (**a**) murine iNOSox and (**b**) human eNOSox, likely due to different positions of the alkyl substituent (position 2 for compound **14**, position 3 for compound **15**). Nonetheless, both compounds bind via bidentate hydrogen bonds to active-site **Glu** and backwall **Trp**. Both compounds are too small to induce the Gln-open conformation and opening of the Gln pocket. Key hydrogen bonds (dots), residues involved in compound binding, and Fo-Fc electron density map contoured at 3 σ (blue mesh) are shown.

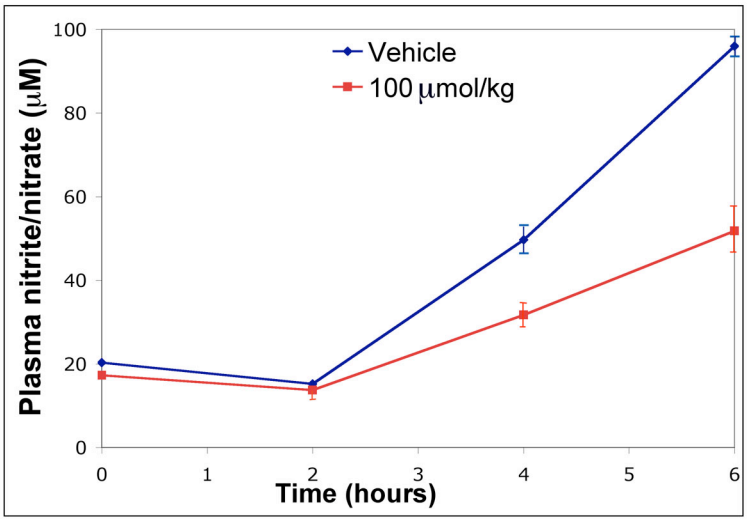

Supplementary Figure 9 Time-course of LPS-induced increases in plasma nitrate/nitrite concentrations in rats. Lipopolysaccharide (LPS) was administered at time zero. Plasma concentrations of nitrate/nitrite were determined at various times (0, 2, 4, and 6 hours). Data are expressed as mean ± standard error; n=3. Blue: control rats (Vehicle), red: inhibitor-dosed rats (Compound **12**).

Supplementary Tables.

Supplementary Table 1. Inhibition potency of N-substituted aminopyridines**.**

No.	Structure	iNOS IC_{50} (μM)	eNOS IC_{50} (μM) (selectivity)	nNOS IC_{50} (μM) (selectivity)
9	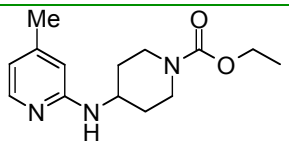	0.35	58 (x166)	20 (x57)
10	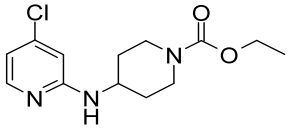	0.72	>100 (x138)	63 (x88)
11	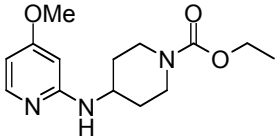	0.09	100 (>x1111)	30 (x333)
12	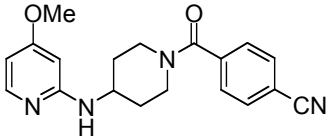	0.074	>100 (>x1351)	6.0 (x81)

Supplementary Table 2. *In vivo* potency of compounds **3** and **12** in whole cells and in the rat model for LPS-induced NO production.

Compound	**iNOS cell IC_{50} (μM)**	**ID_{50} po[b] in rat (4 h postdose) (μmol/kg)**
3[a]	0.9	3
12	1.9	1.8

[a](ref. 2)

[b]Dose that reduces the NO production by 50 %.

Supplementary Table 3. X-ray data collection and refinement statistics for quinazoline complexes

Inhibitor	**1**	**2**	**3**	**4**	**5**
Data collection					
Space group	$P6_122$	$P6_122$	$P6_122$	$P6_122$	$P6_122$
Cell dimensions a, b, c (Å) α, β, γ, (°)	213.9, 213.9, 113.3 90, 90, 120	213.0, 213.0, 115.7 90, 90, 120	214.2, 214.2, 116.9 90, 90, 120	214.0, 214.0, 117.2 90, 90, 120	214.0, 214.0, 116.8 90, 90, 120
Resolution (Å)	2.9 (3.00-2.9)	2.6 (2.7-2.6)	2.6 (2.69-2.6)	2.05 (2.12-2.05)	2.5 (2.59-2.5)
R_{sym} (%)	5.5 (40.8)	8.1 (29.4)	6.4 (40.7)	6.3 (39.8)	4.7 (34.5)
I/σI	37.5 (4)	11.1 (4)	17.3 (2.7)	12 (6)	17.8 (2.5)
Completeness (%)	94.0 (93.3)	99.8 (99.8)	96.2 (93.6)	95.5 (86.0)	96.0 (80.2)
Redundancy	4.5 (3.7)	4 (4)	3 (3)	5.5 (5)	3 (2)
Refinement					
Resolution (Å)	20-2.9	20.0-2.6	20-2.6	20-2.05	20-2.5
No. Reflections	28,329	44,766	44,360	93,821	50,946
R_{work}/ R_{free}	0.239/0.295	0.229/0.262	0.232/0.263	0.249/0.271	0.236/0.267
No. atoms					
Protein	6,848	6,732	6,736	6,816	6,732
Ligand/ion	2 [heme BH4, **Cmp 1**] 1 SO_4	2 [heme BH4 **Cmp 2**]	2 [heme BH4 **Cmp 3**] 1 SO_4	2 [heme BH4 **Cmp 4**]	2 [heme BH4 **Cmp 5**]
Water	191	273	324	149	249
B-factors					
Protein	75.3	46.4	52.6	44.6	53.4
Ligand/ion	62.8	30.5	41.8	31.2	41.8
Water	67.3	40.5	50.0	41.2	45.2
R.m.s. deviations					
Bond lengths (Å)	0.008	0.008	0.008	0.008	0.008
Bond angles (°)	1.4	1.3	1.3	1.3	1.4

Supplementary Table 4. X-ray data collection and refinement statistics for aminopyridines

Inhibitor	**6**	**7**	**8**	**9**[a]	**9**[b]	**9**[c]	**9**[d]	**10**	**12**
Data collection									
Space group	$P6_122$	$P6_122$	$P6_122$	$P6_122$	$P2_12_12_1$	$P2_12_12_1$	$P2_12_12_1$	$P6_122$	$P6_122$
Cell dimensions a, b, c (Å) α, β, γ, (°)	214.1, 214.1, 115.9 90, 90, 120	214.2, 214.2, 112.3 90,90, 120	213.8, 213.8, 115.8 90,90, 120	213.8, 213.8, 116.7 90,90, 120	90.2, 158.7, 191.0 90,90, 90, 90	89.9, 150.7, 191.0 90, 90, 90	58.9, 104.4, 156.7 90, 90, 90	213.9, 213.9, 116.2 90,90, 120	213.1, 213.1, 116.6 90,90, 90, 90
Resolution (Å)	20-2.6 (2.7-2.6)	20-2.4 (2.49-2.4)	20-2.2 (2.28-2.2)	20-2.0 (2.07-2.0)	40-2.1 (2.18-2.1)	50.0-2.55 (2.64-2.55)	30-2.5 (2.6-2.5)	30-2.3 (2.38-2.3)	20-2.2 (2.32-2.2)
R_{sym} (%)	6.8 (17.2)	5.0 (36)	5.4 (42)	3.2 (31.6)	7.7 (32.7)	10.4 (27.4)	8.4 (31)	4.3 (21.6)	6.6 (61.9)
Completeness (%)	81.0 (38)	97.7 (94.7)	96.8 (92.1)	98.7 (96.1)	88.4 (51.1)	92.0 (59.0)	86 (54.2)	97.9 (94)	85.6 (61.3)
I/σI	10 (3)	11.4 (5)	12.4 (3)	20.4 (4)	7.3 (2)	15.6 (3.5)	12 (4)	17.9 (4.6)	8.0 (1.2)
Redundancy	3 (2)	6.9 (6.6)	4 (4)	4 (4)	5.5 (2)	4.3 (2.2)	5 (2.5)	3 (2)	3.1 (2)
Refinement									
Resolution (Å)	20-2.7	20-2.4	20-2.2	20-2.0	40-2.2	100-2.55	30-2.5	30-2.3	20.0-2.2
Reflections	39,090	51,440	76,336	103,993	125,869	85,268	29,456	64,308	67,287
R_{cryst}	0.234	0.233	0.247	0.223	0.182	0.258	0.212	0.219	0.223
R_{free}	0.268	0.270	0.275	0.237	0.213	0.293	0.254	0.244	0.259
No. atoms									
Protein	6,722	6,726	6,732	6,810	13,775	13,775	6,373	6,724	6,848
Ligand/ions	2 [heme BH4 **Cmp 6**]	2 [heme BH4 **Cmp 7**]	2 [heme BH4 **Cmp 8**] 2 βOG 5 SO_4 6 EG	2 [heme BH4 **Cmp 9**] 1 Zn 2 ED	4 [heme BH4 **Cmp 9**] 2 Zn	4 [heme BH4] 2 Zn	2 heme 4 **Cmp 9** 1 Zn 1 CAS	2 [heme BH4 **Cmp 10**] 2 βOG 9 SO_4	2 [heme BH4 **Cmp 12**] 4 SO_4
Water	75	493	570	506	504	275	167	545	831
B-factors									
Protein	59.7	49.2	48.7	35.6	49.6	52.6	28.2	45.6	29.9
Ligand/ion	34.6	28.2	50.6	25.8	38.5	43.4	23.1	54.4	46.2
Water	43.7	52.5	51.0	44.6	46.6	48.0	25.1	47.9	58
R.m.s. deviations									
Bond lengths (Å)	0.009	0.008	0.008	0.007	0.009	0.008	0.009	0.008	0.007
Bond angles (°)	1.3	1.4	1.4	1.3	1.4	1.3	1.8	1.4	1.3

6-8, and 10: murine iNOSox. **9**[a-d] murine iNOSox (a), human iNOSox wild type (b), human iNOSox F286I/L305V (c) mutant and bovine eNOSox (d). **12**. Murine iNOSox.
βOG: β–octyl glucoside, EG: ethylene glycol, ED: ethanediol, CAS: di methyl arsenic cysteine.

Supplementary Table 5. X-ray data collection and refinement statistics for bicyclic thioenooxazepine complexes

Inhibitor	**14**[a]	**15**[b]	**16**[a]
Data collection			
Space group	$P6_122$	$P2_12_12_1$	$P6_122$
Cell dimensions a, b, c (Å) α, β, γ, (°)	213.4, 213.4, 116.1 90, 90, 120	71.1, 90.1, 156.0 90, 90, 90	212.9, 212.9, 116.6 90, 90, 90
Resolution (Å)	20-2.4 (2.53-2.4)	30-2.45 (2.5-2.45)	20-2.28 (2.41-2.28)
R_{sym} (%)	6.6 (49.3)	8.0 (44.5)	5.4 (30.4)
Completeness (%)	90.4 (67.6)	90.9 (84.6)	92.9 (63.8)
I/σI	7.9 (1.5)	7.4 (1.5)	12.2 (2.4)
Redundancy	3.1 (1.8)	2 (1)	3.5 (2.3)
Refinement			
Resolution range (Å)	20-2.4	25-2.44	20-2.28
Reflections	54,713	36,303	65,252
R_{cryst}/R_{free}	0.213/0.247	0.213/0.258	0.201/0.243
No. atoms			
Protein	6,846	6,392	6,846
Ligand/ion	2 [heme BH4 Cmp **14**] 4 SO_4	2 [heme BH4 Cmp **15** MPD Cl] 1 Zn	2 [heme BH4 Cmp **16**] 4 SO_4
Water	796	143	855
B-factors			
Protein	43.9	39.7	33.0
Ligand/ions	33.3	44.2	26.2
Water	54.3	37.9	45.7
R.m.s. deviations			
Bond lengths (Å)	0.006	0.007	0.006
Bond angles (°)	1.3	1.4	1.3

[a]murine iNOSox
[b]bovine eNOSox

Supplementary Results and Discussion.

Quinazolines and aminopyridine binding to iNOSox

Quinazoline inhibitors share a common (di)-fluoro-quinazoline amine core (black in **Fig. 1**), but have different tails (magenta in **Fig. 1**), corresponding to thienyl (**1**), furanamido-ethyl (**2**), cyano-pyridylcarbonyl spiro-piperidinyl (**3**), aminomethyl-benzoyl spiro-piperidinyl (**4**), and cyano-benzoyl spiro-piperidinyl (**5**) moieties. Aminopyridine inhibitors share a 4-methyl-2-aminopyridine core (compound **6**, black in **Fig. 1**) and can either be 6-substituted (**7-8**) or N-substituted (**9-12**). Compounds **7-12** contain a propyl (**7**), 4-cyano-benzamidoethyl (**8**), ethoxycarbonyl-piperidinyl (**9-10**) or 4-cyano-benzoyl-piperidinyl (**12**) tail, reminiscent of the tails found in compounds **1-5**. All compounds bind similarly in the iNOSox active site (Supplementary **Fig. 2a-k**). Small compounds **1** and **6** pack more parallel to the heme than do bulkier compounds **2-5** and **7-12**. The interplanar angle between the inhibitor core and the heme is 6° for compounds **1** and **6** but it averages 13° for quinazolines **2-5**, and 20° for aminopyridines **7-10**. These differences might explain the increased potency of the small compounds for iNOS. Besides the hydrogen bonds to active-site **Glu** and stacking with the heme, compounds **6** and **7** make no further interaction with the protein. However, both compounds are potent iNOS inhibitors, thus highlighting the importance of hydrophobic stacking and hydrogen bonding interactions. Compounds **1-8** make an extra hydrogen bond to Trp366/372 and pack more parallel to the heme plane than compounds **9-12** (average interplanar angles of 13° and 26°, respectively), thus possibly explaining their improved potency in iNOS (**Fig. 1**, **Supplementary Fig. 2**).

We explored permissive substitutions of compound **9** (**Supplementary Table 1**). Changing the 4-methyl group in compound **9** into chlorine (compound **10**) slightly decreases the inhibitor potency in all three isozymes. However, substitution with a 4-methoxy group (compound **11**) improves potency 3 fold against iNOS without affecting potency in the other isoforms, thus contributing to increased isozyme selectivity (1111 fold against eNOS, 333 fold against nNOS). Further elaboration of the piperidine acyl group to a substituted benzamide (compound **12**) affords excellent selectivity against eNOS (1351 fold) and nNOS (81 fold).

Bulky inhibitors induce conformational changes in iNOSox

We superimposed the x-ray structures of murine iNOS bound to N-hydroxy-L-arginine (NOHA, PDB entry 1DWW[1]), small inhibitor **6** and highly selective compounds **3** (ref. 2), **9** (ref. 3), and **12** (ref. 3). The superimposition shows that all structures are very similar (0.4 Å average r.m.s. deviation for all Cα). In the active-site heme pocket, the cis-amidine moieties of the quinazoline (**Supplementary Fig. 3a**) and aminopyridine (**Supplementary Fig. 3b**) inhibitors bind like the NOHA (**Supplementary Fig. 3c**) and L-Arg guanidinium groups[4], via heme stacking and anchoring hydrogen bonds to **Glu**. The NOHA carboxylate group is tethered by hydrogen bonds to Tyr367/373 and **Gln** in the "carboxylate pocket", which was proposed to exclude inhibitors larger than L-Arg or not based on amino acid L-Arg[5]. In the iNOSox complex with intermediate NOHA or small compound **6** (**Fig. 2a**), first-shell **Gln** hydrogen bonds to **Tyr**, and **Arg** hydrogen bonds to Ser256/262 (**Supplementary Fig. 3c**). In contrast, we observe that the longer, rigid and bulky tail

of compound **3** (and compounds **9** and **12**) forms a hydrogen bond from **Tyr** to the inhibitor carbonyl oxygen atom (**Fig. 2b-d**, **Supplementary Fig. 3**). In addition, the side chains of invariant first-shell residues **Gln** (r.m.s.d. value of 3.3 Å), **Arg** (0.6 Å) and Arg382/388 (0.7 Å) show significant changes that lead to the opening of the new Gln specificity pocket in these complexes. In murine iNOS, the **Arg** side-chain rotation is accommodated by the small size of Thr277 and no further compensatory propagation of side-chain movements, like the ones observed in human iNOS, occurs (**Fig. 2**, **Supplementary Fig. 4**). Binding of compound **1**, with its smaller tail, induces smaller rotations of **Gln** and **Arg** and no rotation of Arg382/388, leading to partial opening of the Gln specificity pocket (**Supplementary Fig. 2a**). Importantly, all iNOSox structures in complex with bulky inhibitors bearing rigid extended tails present the Gln-open conformation and corresponding side-chain conformations for **Arg** and Arg382/388 (**Supplementary Fig. 2**). Thus, we predict that these inhibitors will all induce the same cascade of side-chain rotations observed in human iNOSox upon compound **9** binding.

Compound 9 binding to eNOSox and iNOSox

The eNOSox protein overall structure and active site closely resemble those of iNOSox. The structures of eNOSox and iNOSox with compound **9** superimpose with an overall r.m.s. deviation of 0.8 Å (same for both human and murine iNOSox). In eNOS, the anchoring hydrogen bonds to active site **Glu** place the aminopyridine core almost parallel to the heme plane (interplanar angle is ~20° in eNOS vs. 30° in iNOS), and the bulky tail packs between the heme propionates and with conserved

residue Val337/346/352 (**Supplementary Fig. 6**). This position of the rigid inhibitor tail induces slight side-chain rotations of Trp448/457/463 on the propionate A side, and of Tyr476/485/491 on the propionate B side. Thus, both the core and the extended tail of aminopyridine compound **9** interact more closely with the eNOS heme than with the iNOS heme.

Interestingly, in the eNOS:compound **9** complex, the heme is more planar than in iNOS (see below) and a second inhibitor molecule now occupies the pterin site (**Supplementary Fig. 6a**). The aminopyridine core of this second inhibitor molecule lies almost perpendicular to the heme plane, and stacks with pterin-site residue Trp448/457/463 and residue Phe461/470/476 of the adjacent monomer. Additionally, the second inhibitor makes bidentate hydrogen bonds with heme propionate A, mimicking those observed with **Glu** in the active site. The inhibitor tail packs with residues Arg366/375/381 and Val105/Met114/Met120, and Trp75/84/90 from the adjacent monomer. Thus the binding mode of the second inhibitor molecule in the pterin-binding site closely resembles that of H4B[4].

Differences in pterin occupancy between eNOS and iNOS

The second inhibitor molecule in eNOSox mimics H4B binding but cannot substitute for its essential structural, allosteric, and electronic roles[6] in NOS catalysis. The nearly identical pterin-binding sites of the three NOS isozymes exhibit comparable H4B affinities[7], but differing crystallographic occupancies. In eNOS crystal structures, pterin replacement by inhibitor, solvent, cryoprotectant, and substrate is common[8-10],

whereas the H4B sites in iNOS and nNOS x-ray structures are always occupied by pterin[1,11,12] (**Supplementary Tables 3-5**).

Structural comparisons of the NOS isozymes provide insights into the origin of this eNOS peculiarity. In the H4B sites, the π-stacking residues (Trp448/457/463 and Phe461/470/476) and Arg366/375/381 are conserved among isozymes, and most hydrogen bonds are made with main-chain carbonyl oxygen atoms[4]. The only side chains that differ between the eNOS and iNOS H4B sites are Ala447/Ile456/Ile462 (bovine eNOS/murine iNOS/human iNOS numbering) and Val105/Met114/Met120 (corresponding to human nNOS Val682 and Met340, respectively). In iNOS (and nNOS), the bulky Met114 side chain more effectively sequesters pterin from solvent and makes tighter hydrophobic contacts with H4B C4 and N5 atoms than does the smaller Val side-chain in eNOS[13]. Accordingly, the eNOS pterin site can accommodate solvent molecules next to H4B to fill the void left by the smaller Val side chain[14].

The H4B environment in NOS influences the formation and stability of the transient cationic H4B radical, which forms during NO synthesis and is localized predominantly at the N5 position[15,16]. The N5-methyl H4B analog (5Me-H4B), which also supports NO synthesis[17], significantly accelerates radical formation and greatly enhances radical stability in all three isozymes[18]. Comparison of the murine iNOS x-ray structures bound to 5Me-H4B vs. H4B shows no major structural differences[19], but reveals that the bulky Met114 thiomethyl group packs closer to 5Me-H4B. Among the three NOS isozymes, eNOS, which lacks this thiomethyl, presents the slowest formation and the fastest decay rates for the H4B radical[18]. Isozyme-specific

differences in the pterin-binding site of NOS may also facilitate H4B exchange in eNOS. Comparisons of the iNOS and eNOS complexes with aminopyridine compound **9** (**Supplementary Fig. 6**) suggest isozyme-specific differences in both the H4B and L-Arg binding sites that could impact H4B replacement. In the H4B site, the bulky Met side-chain in iNOS (and nNOS) may preclude eNOS-like inhibitor binding. In the L-Arg site, the packing of the rigid and bulky compound **9** tail between the heme propionates in eNOS is associated with shifts in conserved Trp448/457/463, which is important for stabilizing H4B binding[11]. Thus, our studies prompt the hypotheses that (i) the increased openness and solvent accessibility of the eNOS pterin site and/or (ii) aminopyridine binding in the eNOS active site facilitates inhibitor replacement of H4B. Regardless of the mechanism, aminopyridine binding to eNOS likely inhibits NO synthesis by disrupting H4B binding.

Differences in heme planarity between eNOS and iNOS

From structural comparisons of iNOS and eNOS bound to aminopyridine compound **9** (**Supplementary Fig. 6**) and other inhibitors, we found the eNOS heme to be more planar and less distorted than its iNOSox counterpart. To quantify the degree of heme distortion in NOSox structures, we applied the normal-coordinate structural decomposition method[20], which classifies heme distortions into low-energy vibrational modes including ruffling, saddling, doming, waving, and pyrrole propellering deformations. In iNOSox complexes with compounds **1-10**, we found that the average heme out-of-plane distortion is 0.8 Å vs. 0.5 Å in 20 eNOSox structures (our unpublished results). In the compound **9** complexes reported here, the average heme

out-of-plane distortion is again significantly greater in iNOSox (1.0 Å) than in eNOSox (0.6 Å; Methods). Our results indicate that all NOS isozymes exhibit significantly distorted heme conformations. In other heme-containing proteins, even lesser distortions have been shown to tune optical and redox properties, and thus play significant biological roles[21]. In NOS, distortional differences of the heme among the three isozymes may be linked to different coupling interactions of heme with pterin and different degrees of NOS self-inhibition by the product NO[22,23], and thus have important implications for isozyme-specific regulation.

The double human iNOSox mutant mimics eNOSox

To test the role of isozyme-specific third-shell residues, we mutated human iNOSox Phe286 into Ile and Val305 into Leu to mimic human eNOSox. Human iNOSox carrying the double mutation Phe286Ile/Val305Leu exhibited the UV-visible spectral properties of wild-type human iNOSox, indicating that these mutations do not perturb enzyme structure or the heme electronic environment. To confirm this result, we determined the x-ray structure of the human iNOSox double mutant (Methods) co-crystallized with excess compound **9** (55-fold molar excess), and showed that the Gln specificity pocket and inhibitor are not present (**Supplementary Fig. 7**).

Supplementary Methods

Synthesis of Compounds 13-16

Compound **15a**: tert-Butyl N-(1-hydroxypentan-2-yl)carbamate

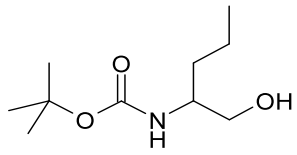

(R,S)-2-Aminopentanol (9.25 g, 90 mmol) was dissolved in dry tetrahydrofuran (100 ml) and treated with pyridine (7.9 g, 100 mmol). The solution was cooled in an ice bath and stirred under a nitrogen atmosphere. Di-*tert*-butyldicarbonate (19.6 g, 90mmol) was added and the mixture was allowed to warm up to ambient temperature over 18hr with stirring. The mixture was poured into aqueous 2 M hydrochloric acid and the product was extracted using ethyl acetate. The ethyl acetate was removed under reduced pressure to give the product **15a** as a clear oil (16.7 g).

Mass spectrum: m/e 202 [M-H].
^{1}H NMR: δ $CDCl_3$ 0.93 (t, 3H), 1.33-1.44 (m, 4H), 1.45 (s, 9H), 2.57 (bs, 1H), 3.50-3.56 (m, 1H), 3.65-3.69 (m, 2H), 4.62 (bs, 1H).

Compound **15b**: Methyl 3-[2-[(2-methylpropan-2-yl)oxycarbonylamino]pentoxy]thiophene-2-carboxylate

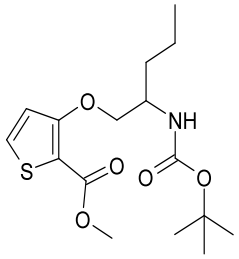

Methyl 3-hydroxythiophene-2-carboxylate (1.58 g, 10 mmol), triphenylphosphine (2.62 g, 10 mmol) and compound **15a** (2.03 g, 10 mmol) were dissolved in dry benzene (25 ml) and stirred under a nitrogen atmosphere. Diethyl azodicarboxylate (1.74 g, 10 mmol) was added and the mixture stirred for 3hr at ambient temperature. The reaction mixture was absorbed onto silica and passed down a silica gel column eluted with hexane:ethyl acetate (4:1) to yield the product **15b** (2.8 g).

Mass spectrum: m/e 244 [M-Boc].

^{1}H NMR: δ $CDCl_3$ 0.95 (t, 3H), 1.38-1.42 (m, 2H), 1.44 (s, 9H), 1.65-1.71 (m, 2H), 3.85 (s, 3H), 3.87-3.90 (m, 1H), 4.10-4.18 (m, 2H), 5.12 (bs, 1H), 6.85 (d, 1H), 7.40 (d, 1H).

Compound **15c**: Methyl 3-(2-aminopentoxy)-thiophene-2-carboxylate Hydrochloride.

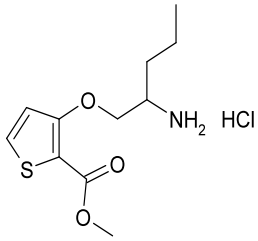

Compound **15b** (2.8 g, 8.2 mmol) was dissolved in 4M hydrochloric acid in dioxane (25 ml) and stirred for 2 hr. The solvent was removed under reduced pressure to give compound **15c** (2.3 g) as a gum used in next step without further purification.

Mass spectrum: m/e 244 [M+H].

Compound **15d**: 3-Propyl-3,4-dihydro-2H-thieno[2,3-f][1,4]oxazepine-5-one

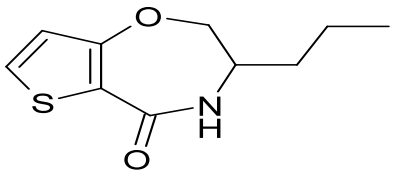

Compound **15c** (2.3 g, 8 mmol) and 1,8-diazabicyclo[5.4.0]undec-7-ene (3 g, 20 mmol) were dissolved in dimethylformamide (50 ml) and heated at 110 °C for 24 hr. The reaction mixture was poured into 2 M hydrochloric acid and extracted with ethyl acetate, which was evaporated under reduced pressure to give a gum. This mixture crystallized from hexane/ethyl acetate to give compound **15d** as a white solid (1.1 g).

Mass spectrum: m/e 212 [M+H].

^{1}H NMR: δ $CDCl_3$ 0.97 (t, 3H), 1.44-1.53 (m, 2H), 1.54-1.65 (m, 2H), 3.53-3.60 (m, 1H), 4.24-4.35 (m, 2H), 6.33 (bs, 1H), 6.87 (d, 1H), 7.38 (d, 1H).

Compound **15e**: 3-Propyl-3,4-dihydro-2H-thieno[2,3-f][1,4]oxazepine-5-thione.

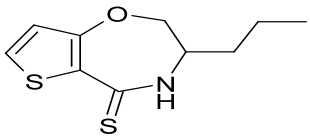

Compound **15d** (1 g, 4.5 mmol) and [2,4-bis(4-methoxyphenyl)-1,3-dithia-2,4diphosphetane-2,4-disulfide] (1.2 g, 3 mmol) in benzene (50 ml) were heated at reflux for 3 hr. The reaction mixture was absorbed onto silica and passed down a silica gel column eluted with hexane:ethyl acetate (4:1) to yield compound **15e** as a yellow solid, (0.77 g), used directly in the next step.

Mass spectrum: m/e 228 [M+H].

Compound **15f**: 3-Propyl-2,3-dihydro-5-(methylthio)-thieno[2,3-f][1,4]oxazepine hydroiodide.

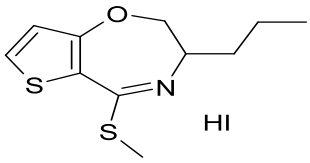

Compound **15e** (0.76 g, 3.3 mmol) was dissolved in acetonitrile (25 ml), treated with methyl iodide (3 g) and stirred at ambient temperature for 20 hr. The reaction mixture was evaporated to dryness yield compound **15f** as a yellow solid (1.2 g), used directly in the next step.

Mass spectrum: m/e 242 [M+1].

Compound **15**: 3-Propyl-2,3-dihydrothieno[2,3-f][1,4]oxazepin-5-amine Hydrochloride.

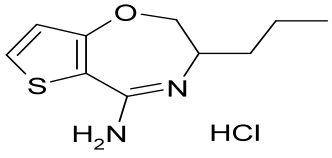

Compound **15f** (1.2 g, 3.25 mmol) and ammonium acetate (2.5 g, 33 mmol) in acetonitrile (25 ml) were heated at reflux for 6hr. The mixture was poured into water (150 ml) and extracted with ethyl acetate. The aqueous layer was then basified with 2M NaOH to pH>12 and extracted with ethyl acetate (3 x 200 ml). The combined extracts were washed with saturated sodium bicarbonate, brine, dried over anhydrous $MgSO_4$ and evaporated under reduced pressure to give a white solid. This solid was stirred with 1 M ethereal hydrochloric acid to yield compound **15** as a white solid (0.51 g).

M.p.: 223-4 °C.

Mass spectrum: m/e 211 [M+H].

^{1}H NMR: δ $DMSO_{d6}$ 0.90 (t, 3H), 1.46-1.55 (m, 4H), 3.85 (m, 1H), 4.45 (m, 2H), 6.96 (d, 1H), 8.08 (d, 1H), 8.65 (bs, 2H), 10.25 (bs, 1H).

CHN Analysis: $C_{10}H_{15}N_2ClOS$ requires: C 48.67 H 6.13 N 11.35 S 12.99 %

found: C 48.86 H 6.12 N 11.40 S 12.56 %

Compound **14**: (2S)-2-Methyl-2,3-dihydrothieno[2,3-f][1,4]oxazepin-5-amine Hydrochloride

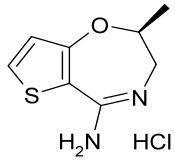

Compound **14** was synthesized via the route described for compound **15**, by starting with (R)-1-amino-2-propanol.

M.p.: 210-2 °C.

Mass spectrum: m/e 183 [M+H].

^{1}H NMR: δ $DMSO_{d6}$ 1.48 (d, 3H), 3.45-3.52 (m, 1H), 3.75-3.85 (m, 1H), 4.48-4.55 (m, 1H), 6.77 (d, 1H), 7.62 (d, 1H), 7.8 (bs, 1H), 9.0 (bs, 1H) 10.9 (bs, 1H).

CHN Analysis $C_8H_{11}N_2ClOS$ requires: C 43.9 H 5.1 N 12.8 S 14.7 %

found: C 43.8 H 5.1 N 12.6 S 14.5 %

Compound **13**: 2,3-Dihydrothieno[2,3-f][1,4]oxazepin-5-amine Hydrochloride

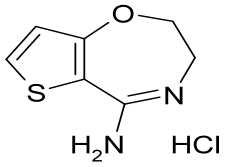

Compound **13** was synthesized via the route described for compound **15**, by starting with 2-aminoethanol. The product was isolated as a monohydrate.

M.p.: 113-4 °C.

Mass spectrum: m/e 169 [M+H].

^{1}H NMR: δ $DMSO_{d6}$ 3.79 (m, 2H), 4.50 (m, 2H), 6.81 (d, 1H), 7.70 (d, 1H), 8.7(bs, 2H), 10.9 (bs, 1H)

CHN Analysis $C_7H_9N_2ClOS.H_2O$ requires: C 37.8 H 5.0 N 12.6 S 14.4 %

found: C 38.0 H 5.1 N 12.5 S 14.1 %

Compound **16a**: 3-(Hydroxymethyl)-3,4-dihydro-2H-thieno[2,3-f][1,4]oxazepin-5-one

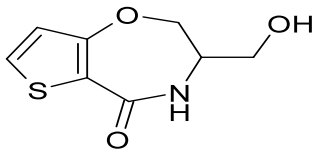

Compound **16a** was synthesized via the route described for compound **15c** by starting with 2-amino-1,3-propanediol.

Mass spectrum: m/e 199 [M+H].

Compound **16b**: tert-Butyl 7-[(5-oxo-3,4-dihydro-2H-thieno[2,3-f][1,4]oxazepin-3-yl)methoxy]-3,4-dihydro-1H-isoquinoline-2-carboxylate

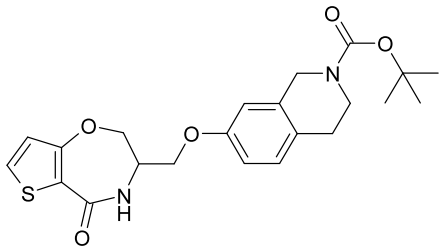

Product **16a** (1.09 g, 5.5 mmol) and tert-butyl 7-hydroxy-3,4-dihydro-2-(1H)isoquinoline carboxylate (1.27 g, 5.1 mmole: *J. Med. Chem.* (1998), **41**, 4983-4994) were coupled using the Mitsunobu reaction via the method as described in example **15b** to give the title compound **16b** as a colorless gum (0.43 g, 20 %).

Mass spectrum: m/e 331 [M+H-Boc].
δ $CDCl_3$ 1.49 (s, 9H), 2.74-2.78 (m, 2H), 3.60-3.64 (m, 2H), 3.97-4.04 (m, 2H), 4.10-4.17 (m, 1H), 4.40-4.58 (m, 4H), 6.50 (bd, s, 1H), 6.64 (s, 1H), 6.68-6.75 (m, 2H), 7.05 (d, 1H) and 7.41 (d, 1H).

Compound **16c**: tert-Butyl 7-[(5-sulfanylidene-3,4-dihydro-2H-thieno[2,3-f][1,4]oxazepin-3-yl)methoxy]-3,4-dihydro-1H-isoquinoline-2-carboxylate

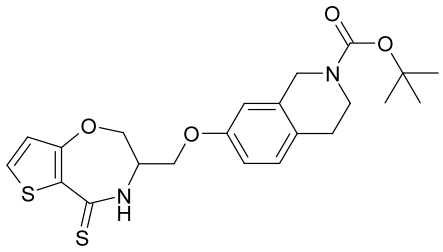

Product **16b** (55 mg, 0.16 mmol) was converted to the title compound **16c** using Lawessons reagent via the method as described in example **15e**.

Mass spectrum: m/e 347 [M+H-Boc].
δ $CDCl_3$ 1.49 (s, 9H), 2.74-2.78 (m, 2H), 3.60-3.64 (m, 2H), 4.08-4.18 (m, 3H), 4.43-4.53 (m, 4H), 6.64 (s, 1H), 6.67-6.75 (m, 2H), 7.05 (d, 1H) and 7.49 (d, 1H), 8.62 (bd. s, 1H).

Compound **16**: 3-(1,2,3,4-Tetrahydroisoquinolin-7-yloxymethyl)-2,3-dihydrothieno[2,3-f][1,4]oxazepin-5-amine Dihydrochloride.

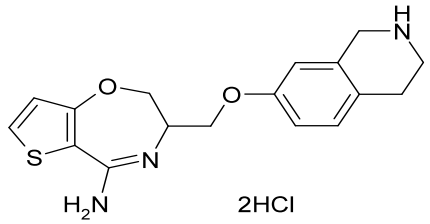

Product **16c** (53 mg, 0.09 mmol) was converted directly to the title compound via the method described in example **15f** and **15** with deprotection of the silyl group being effected with 5 M hydrochloric acid in dioxane to yield compound **16** as a dihydrochloride salt.

M.p.: 197-8 °C.

Mass spectrum: m/e 330 [M+H].

^{1}H NMR: δ $DMSO_{d6}$ 2.90-2.95 (m, 2H), 3.34-3.38 (m, 2H), 4.10-4.34 (m, 5H), 4.61-4.65 (m, 2H), 6.86-6.90 (m, 2H), 6.98 (d, 1H), 7.15 (d, 1H), 8.11 (d, 1H) 8.72 (bs, 2H), 9.37 (bs, 2H), 10.16 (v bs, 1H).

Supplementary Movie 1 Legend

The Quicktime movie illustrates the cascade of conformational changes that occur in human iNOSox upon aminopyridine compound **9** binding (Quicktime, 582 kB).

Supplementary references.

1. Crane, B.R. *et al.* Structures of the N(omega)-hydroxy-L-arginine complex of inducible nitric oxide synthase oxygenase dimer with active and inactive pterins. *Biochemistry* **39**, 4608-4621 (2000).
2. Tinker, A.C. *et al.* 1,2-dihydro-4-quinazolinamine: potent, highly selective inhibitors of inducible nitric oxide synthase which show antiinflammatory activity in vivo. *J. Med. Chem.* **46**, 913-916 (2003).
3. Connolly, S. *et al.* 2-aminopyridines as highly-selective inducible nitric oxide synthase inhibitors. Differential binding modes dependent on nitrogen substitution. *J. Med. Chem.* **47**, 3320-3323 (2004).
4. Crane, B.R. *et al.* Structure of nitric oxide synthase oxygenase dimer with pterin and substrate. *Science* **279**, 2121-2126 (1998).
5. Li, H. & Poulos, T.L. Structure-function studies on nitric oxide synthases. *J. Inorg. Biochem.* **99**, 293-305 (2005).
6. Werner, E.R., Gorren, A.C.F., Heller, R., Werner-Felmayer, G. & Mayer, B. Tetrahydrobiopterin and nitric oxide: mechanistic and pharmacological aspects. *Exp. Mol. Med.* **228**, 1291-1302 (2003).
7. Wei, C.-C., Crane, B.R. & Stuehr, D.J. Tetrahydrobiopterin radical enzymology. *Chem. Rev.* **103**, 2365-2383 (2003).
8. Fischmann, T.O. *et al.* Structural characterization of nitric oxide synthase isoforms reveals striking active-site conservation. *Nat. Struct. Biol.* **6**, 233-242 (1999).
9. Rosenfeld, R.J. *et al.* Conformational changes in nitric oxide synthases induced by chlorzoxazone and nitroindazoles: crystallographic and computational analyses of inhibitor potency. *Biochemistry* **41**, 13915-13925. (2002).
10. Raman, C.S. *et al.* Crystal structure of nitric oxide synthase bound to nitroindazole reveals a novel inactivation mechanism. *Biochemistry* **40**, 13448-13455 (2001).
11. Aoyagi, M. *et al.* Structures of tetrahydrobiopterin binding-site mutants of inducible nitric oxide synthase oxygenase dimer and implicated roles of Trp457. *Biochemistry* **40**, 12826-12832 (2001).
12. Fedorov, R., Vasan, R., Ghosh, D.K. & Schlichting, I. Structures of nitric oxide synthase isoforms complexed with the inhibitor AR-R17477 suggest a rational basis for specificity and inhibitor design. *Proc. Nat. Acad. Sci. USA* **101**, 5892-5897 (2004).
13. Li, H. *et al.* Crystal structures of zinc-free and -bound heme domain of human inducible nitric-oxide synthase. Implications for dimer stability and comparison with endothelial nitric-oxide synthase. *J. Biol. Chem.* **274**, 21276-84 (1999).
14. Flinspach, M. *et al.* Structures of the neuronal and endothelial nitric oxide synthase heme domain with D-nitroarginine-containing dipeptide inhibitors bound. *Biochemistry* **43**, 5181-5187 (2004).
15. Hurshman, A.R., Krebs, C., Edmondson, D.E., Huynh, B.H. & Marletta, M.A. Formation of a pterin radical in the reaction of the heme domain of inducible nitric oxide synthase with oxygen. *Biochemistry* **38**, 15689-15696 (1999).

16. Schmidt, P.P. *et al.* Formation of a protonated trihydrobiopterin radical in the first reaction cycle of neuronal and endothelial nitric oxide synthase detected by electron paramagnetic resonance spectroscopy. *J. Inorg. Chem.* **6**, 151-158 (2001).
17. Gorren, A.C. *et al.* Nitric oxide-induced autoinhibition of neuronal nitric oxide synthase in the presence of the autooxidation-resistant pteridine 5-methyltetrahydrobiopterin. *Biochem. J.* **347**, 475-484 (2000).
18. Wei, C.-C. *et al.* The three nitric-oxide synthases differ in their kinetics of tetrahydrobiopterin radical formation, heme-dioxy reduction, and arginine hydroxylation. *J. Biol. Chem.* **280**, 8929-8935 (2005).
19. Wei, C.-C. *et al.* Structure of tetrahydrobiopterin tunes its electron transfer to the heme-dioxy intermediate in nitric oxide synthase. *Biochemistry* **42**, 1969-1977 (2003).
20. Jentzen, W., Ma, J.-G. & Shelnutt, J.A. Conservation of the Conformation of the Porphyrin Macrocycle in Hemoproteins. *Biophys. J.* **74**, 753-763 (1998).
21. Shelnutt, J.A. *et al.* Nonplanar porphyrins and their significance in proteins. *Chem. Soc. Rev.* **27**, 31-41 (1998).
22. Santolini, J., Adak, S., Curran, C.M. & Stuehr, D.J. A kinetic simulation model that describes catalysis and regulation in nitric oxide synthase. *J. Biol. Chem.* (2000).
23. Rousseau, D.L., Li, D., Couture, M. & Yeh, S.-R. Ligand-protein interactions in nitric oxide synthase. *J. Inorg. Chem.* **99**, 306-323 (2005).